TECHNICAL ARTICLE

Fundamentals of silico-ferrite of calcium and aluminium (SFCA) and SFCA-I iron ore sinter bonding phase formation: effects of mill scale addition

Nathan A. S. Webster,[1,a] Mark I. Pownceby,[1] and Rachel Pattel[1]
[1]*CSIRO Mineral Resources, Private Bag 10, Clayton South, VIC 3169, Australia*

(Received 6 April 2017; accepted 18 June 2017)

The thermal decomposition of mill scale, and the effect of mill scale addition on the formation and decomposition of Silico-Ferrite of Calcium and Aluminium (SFCA) and SFCA-I iron ore sinter bonding phases, has been investigated using *in situ* X-ray diffraction. Application of the external standard method of quantitative phase analysis of the *in situ* data collected during decomposition of the mill scale highlighted the applicability of this method for the determination of the nature and abundance of amorphous material in a mineral sample. Increasing mill scale addition from 2.6 to 10.6 and to 21.2 wt% in an otherwise synthetic sinter mixture composition designed to form SFCA did not significantly affect the thermal stability ranges of SFCA-I or SFCA, nor did it significantly affect the amount of each of SFCA or SFCA-I, which formed. This was attributed to the low impurity (i.e. Mn, Mg) concentration in the mill scale, and also the transformation to hematite during heating of the wüstite and magnetite present in the mill scale, with the hematite available for reaction to form SFCA and SFCA-I. © *2017 International Centre for Diffraction Data.*
[doi:10.1017/S088571561700080X]

Key words: iron ore sinter, mill scale, SFCA and SFCA-I, formation mechanisms, *in situ* X-ray diffraction

I. INTRODUCTION

"SFCA" (Silico-Ferrite of Calcium and Aluminium) phases are key bonding materials of industrial iron ore sinter. Sinter is a major feedstock material of blast furnaces, utilised extensively worldwide in the production of steel from iron ore. During the iron ore sintering processes, iron ore fines (the <6.3 mm fraction of iron ore) are mixed with flux [e.g. limestone, $CaCO_3$, and usually also dolomite, $CaMg(CO_3)_2$, or other Mg-bearing minerals such as olivine, $(Fe,Mg)_2SiO_4$, and serpentine $(Mg,Fe)_3Si_2O_5(OH)_4$] and coke breeze and heated rapidly (~4 min) to temperatures of ~1300 °C followed by slower cooling in air (Dawson *et al*., 1985). This results in partial melting and the formation of a porous but physically strong composite material in which the iron-bearing minerals hematite, Fe_2O_3, and magnetite, Fe_3O_4 (including relict ore particles) are bonded by a complex matrix containing predominantly "SFCA" phases, as well as other Ca-rich ferrite phases, calcium silicates and glass (quenched liquid).

The "SFCA" in iron ore sinter has been categorised on the basis of composition, morphology, and crystal structure into two main types. The first is a low-Fe form called SFCA, which typically contains 60–76 wt% Fe_2O_3, 13–16 wt% CaO, 3–10 wt% SiO_2, and 4–10 wt% Al_2O_3 (Hancart *et al*., 1967; Ahsan *et al*., 1983). The second is a high-Fe, low-Si (e.g. 84 wt% Fe_2O_3, 13 wt% CaO, 1 wt% SiO_2, and 2 wt% Al_2O_3) form called SFCA-I (Mumme *et al*., 1998). The crystal structures of SFCA and SFCA-I are distinct (Hamilton *et al*., 1989; Mumme *et al*., 1998). A number of recent investigations have utilised *in situ* powder diffraction techniques – laboratory-based X-ray diffraction (XRD), synchrotron XRD, and neutron diffraction – in order to determine the formation mechanisms of SFCA and SFCA-I under simulated sintering conditions (Webster *et al*., 2012, 2013a, 2013b, 2014, 2017).

Sintering technology can also be applied to unconventional sources of ferrous materials including low-grade iron ore (e.g. titanium-rich ironsands) or by-products from iron and steel making processes such as mill scale and collected dusts. In a recent series of publications by Wang *et al*. (2016a) and Webster *et al*. (2016), the effects of New Zealand titanomagnetite ironsand – containing 7.9 wt% Ti – addition on the formation of SFCA and SFCA-I iron ore sinter bonding phases was determined. Ironsand is a relatively cheap source of iron, and the introduction of a minor amount of titanium-bearing ore into the blast furnace burden has been demonstrated to extend blast furnace operating campaigns because of the formation of titanium carbonitrides on the hearth lining (Li *et al*., 2001). Increasing ironsand addition from 1.3 to 6.7 and to 13.8 wt% in an otherwise synthetic sinter mixture composition designed to form SFCA-I did not significantly affect the thermal stability range of SFCA-I, nor did it significantly affect the maximum concentration of SFCA-I attained. The main effect of ironsand addition was a small reduction in the thermal stability range of another complex calcium-rich ferrite, γ-CFF (nominal composition $Ca_{3.0}Fe_{14.82}O_{25}$). In comparison, increasing ironsand addition from 2.4 to 3.9 and to 11.6 wt% in an otherwise synthetic sinter mixture composition designed to form SFCA resulted in a

[a]Author to whom correspondence should be addressed. Electronic mail: nathan.webster@csiro.au

decrease in the maximum SFCA-I concentration, with a corresponding increase in the concentration of SFCA. Separate phase equilibria studies revealed that SFCA can incorporate more titanium in its structure (up to 1.2 wt% TiO_2) than SFCA-I (0.6 wt% TiO_2), which was thought to explain the behaviour in the mixtures designed to form SFCA.

The current paper concerns the effects of adding another unconventional source of iron, mill scale. Mill scale is an Fe-rich (65–70% Fe) waste product containing wüstite (FeO), magnetite and hematite, which is formed on the surface of steel as a result of oxidation during continuous casting, reheating, and hot-rolling operations (Birks *et al*., 2006). Mill scale is often recycled through the sintering process with the exothermic oxidation of wüstite and magnetite providing a reduction in the coke breeze addition (Umadevi *et al*., 2012). Here, the effect of mill scale addition on the formation of SFCA and SFCA-I under simulated sintering conditions is investigated using *in situ* XRD. As part of the study the thermal decomposition of mill scale was also characterised in order to understand how its breakdown may influence the formation of SFCA and SFCA-I during heating.

II. EXPERIMENTAL

A. Sample preparation

The mill scale has previously been characterised (Wang *et al*., 2016b). In summary, its bulk composition is 71.0 wt% total Fe, 0.2 wt% CaO, 0.1 wt% Al_2O_3, 0.9 wt% SiO_2, 0.2 wt% MgO, and 0.6 wt% Mn. Its relative crystalline mineral phase composition determined by XRD is 53 wt% wüstite, 35 wt% magnetite, 10 wt% hematite, and 1 wt% goethite (minor green rust, $Fe_2O_3.H_2O$, also observed). The mill scale was added in progressively higher amounts to fine grained (<20 μm) synthetic Fe_2O_3 (Acros Organics, 99.999% purity), calcite, $CaCO_3$ (Thermo Fisher, 99.95%), quartz, SiO_2 (Sigma Aldrich, 99.995%), and gibbsite, $Al(OH)_3$ (Alcan OP25 Super White, 99.9%), which were mixed under acetone in a mortar and pestle with an intermediate drying and remixing stage to ensure homogenisation. Three sinter mixtures were prepared, with mill scale contents of 2.6–10.6 and to 21.2 wt%. Each mixture had bulk composition – 77.36 wt% Fe_2O_3, 14.08 wt% CaO, 3.56 wt% SiO_2, and 5 wt% Al_2O_3 – matching that of the bulk composition investigated in detail previously by Webster *et al*. (2012, 2013a, 2014, 2016), and within the SFCA compositional stability domain established by Patrick and Pownceby (2001) (i.e. each mixture was designed to form SFCA during heating).

B. *In situ* XRD data collection

Details of the *in situ* XRD experimentation have been described in detail previously (Webster *et al*., 2013a, 2013b, 2016, 2017). The mill scale sample, and the three sinter mixture samples were heated over the range 20–1350 °C, at a heating rate of 20 °C min^{-1} from 20 to 600 °C as the decomposition temperature of $CaCO_3$ was approached, and with individual datasets collected for 1 min continuously during heating. The rate was then reduced to 10 °C min^{-1} for the range 600–1350 °C, which corresponded to the period of Ca-rich ferrite phase formation, reaction and decomposition for the sinter mixture samples. Samples were heated under a flow of a 0.5 vol% O_2 in N_2 gas mixture (to give a nominal oxygen partial pressure of $pO_2 = 5 \times 10^{-3}$ atm). The oxygen partial pressure has been used in all of our *in situ* XRD work, and the selection was based on the work of Hsieh and Whiteman (1989) who determined that this pO_2 maximised the formation of Ca-rich ferrites whilst still producing mineral assemblages similar to those found in industrial sinters.

C. *In situ* XRD data analysis

Rietveld refinement-based QPA was performed using TOPAS (Bruker, 2014). The crystal structure data of Blake *et al*. (1966), Hamilton (1958), Fjellvåg *et al*. (1996), Hazemann *et al*. (1991), and Lager *et al*. (1982) were used for Fe_2O_3, Fe_3O_4, FeO, FeOOH and SiO_2, respectively. Corrections to account for sample displacement and peak intensity variation in asymmetric diffraction geometry were incorporated into the TOPAS refinement. The use of the Hill and Howard QPA algorithm (Hill and Howard, 1987) embodied in TOPAS returns relative, rather than absolute, concentrations for crystalline phases in a system if amorphous material, including melt phases, are present. The previous *in situ* work performed in this context has demonstrated amorphous Al_2O_3 is present in these systems after the decomposition of $Al(OH)_3$. Therefore, absolute phase concentrations as a function of temperature were determined using the "external standard" approach given by Webster *et al*. (2013b)

$$W_i = \frac{\mu_m S_i (ZMV)_i}{K} \quad (1)$$

Here W_i is the weight fraction of phase i, S_i is the Rietveld scale factor, ZM is the unit-cell mass, V is the unit-cell volume, and μ_m is the mass absorption coefficient of the entire mixture. K is an experiment constant used to put W_i on an absolute basis. It was calculated using the "known" concentrations of phases in the starting sample (the assumption is made that the sample is 100% crystalline), and the Rietveld-refined S values for phases in the sample in the first dataset collected at 20 °C according to

$$K = \frac{\mu_m \sum_{i=1}^{n} S_i (ZMV)_i}{\sum_{i=1}^{n} W_i} \quad (2)$$

D. *Ex situ* XRD data collection and analysis

Ex situ XRD data were collected on the mill scale sample, mixed in a 50:50 wt ratio with a very high purity and highly crystalline corundum (α-Al_2O_3; Baikalox Alumina Polishing Powder), over the range 5°–140°2θ using a PANalytical MPD instrument fitted with a cobalt long-fine-focus X-ray tube operated at 40 kV and 40 mA. The incident beam path was defined using 0.04 radian Soller slits, a 20 mm mask, a 0.5° fixed divergence slit, and a 1° anti-scatter slit. The diffracted beam incorporated a second set of Soller slits, a graphite monochromator to eliminate unwanted wavelengths and a 4.6 mm anti-scatter slit. An X'Celerator detector was used in scanning line (1D) mode with an active length of 2.122°2θ. Quantitative phase analysis was performed using the internal

https://doi.org/10.1017/S088571561700080X Published online by Cambridge University Press

standard method (Madsen and Scarlett, 2008), in order to calculate the amorphous content of the mill scale.

III. RESULTS AND DISCUSSION

A. Thermal decomposition of mill scale

Figure 1 shows a plot of accumulated *in situ* XRD data, viewed down the intensity axis and with temperature plotted vs. 2θ, for the experiment performed just using the mill scale sample. Figure 2 shows the results of the Rietveld-based QPA on these *in situ* XRD data, showing absolute phase concentrations as a function of temperature. Based on known phase equilibria between hematite/magnetite and magnetite/wüstite at a pO_2 of 5×10^{-3} atm, magnetite should be the stable Fe-oxide phase between about 1180 and 1750 °C (Huebner, 1971). Wüstite begins transforming first to magnetite at temperatures as low as ~300 °C. At these low temperatures, even though the pO_2 is at 5×10^{-3} atm, the Fe-oxide stability field is for hematite. As the temperature is further increased, the hematite is transformed to magnetite with a transition beginning above 1150 °C and being completed by 1300 °C. Graininess of this Fe_3O_4 above 1250 °C results in poor particle statistics, which has an influence on the QPA in this region.

What is striking about the QPA plot is that the calculated absolute Fe_2O_3 concentration at 850 °C, which is after all of the crystalline FeO and Fe_3O_4 has oxidised, is 133 wt% and greater than was expected (106 wt%) from the sample gaining oxygen during heating. This means that there is unaccounted-for amorphous material in the mill scale sample at room temperature, which crystallises during heating. The results of the internal standard-based determination outlined in the section IID confirm this. Since the mill scale sample exhibited negligible loss on ignition (Wang *et al.*, 2016b) this amorphous material is considered likely to be amorphous/nanocrystalline Fe-oxide material, rather than hydrated mineral(s). This work demonstrates the power of *in situ* XRD, combined with the external standard approach to QPA, for gaining insights into the quantity and nature of amorphous material in mineral mixtures.

Another noteworthy feature of the data shown in Figure 1 is the shift of the FeO reflections to lower 2θ (i.e. unit cell expansion) as this phase converts to Fe_3O_4. This is considered to indicate that the wüstite at room temperature is non-stoichiometric (i.e. $Fe_{1-x}O$), since the lattice parameter of $Fe_{1-x}O$ is smaller than that of FeO (Minervini and Grimes, 1999). The wüstite appears to become more stoichiometric as it converts to Fe_3O_4 during heating. A small shift to higher 2θ (i.e. unit cell contraction) as the FeO converts to Fe_2O_3 is attributed to the smaller size of Fe^{3+} relative to Fe^{2+} (Shannon, 1976).

B. Effects of mill scale addition on SFCA-I and SFCA formation

Figure 3 shows the plot of accumulated *in situ* XRD data for the 21.2 wt% mill scale mixture. Reflections for Fe_2O_3, Fe_3O_4, $Fe_{1-x}O$, $CaCO_3$, α-SiO_2, and $Al(OH)_3$ were observed at room temperature. The first event during heating (note that only the events distinct from those discussed in the section IIIA are discussed here) was the decomposition of $Al(OH)_3$ to amorphous Al-oxide, which was complete by ~300 °C. Then, $CaCO_3$ decomposed to CaO, which was complete by ~680 °C. The first Ca-rich ferrite to form was alumina-substituted dicalcium ferrite [designated hereafter as $C_2(F_{1-x}A_x)$ at ~800 °C, followed by CF (i.e. monocalcium ferrite, where C = CaO and F = Fe_2O_3] and CFA (a phase with average composition 71.7 mass% Fe_2O_3, 12.9 mass% CaO, 0.3 mass% SiO_2, and 15.1 mass% Al_2O_3) (Webster *et al.*, 2012) at ~960 °C. As the temperature increased further, SFCA-I and SFCA formed at ~1110 and 1160 °C, respectively. Melting, which was complete by ~1260 °C, produced a phase assemblage of Fe_3O_4 in a Fe_2O_3–(Fe_3O_4)–CaO–SiO_2–Al_2O_3-rich melt. Each of these temperatures is consistent with those reported by Webster *et al.* (2012) for the mixture SM4/5, which had the same bulk composition as the 21.2 wt% mill scale mixture analysed here, but did not contain mill scale. This suggests that the addition of mill scale has minimal effect of the formation of SFCA-I and SFCA.

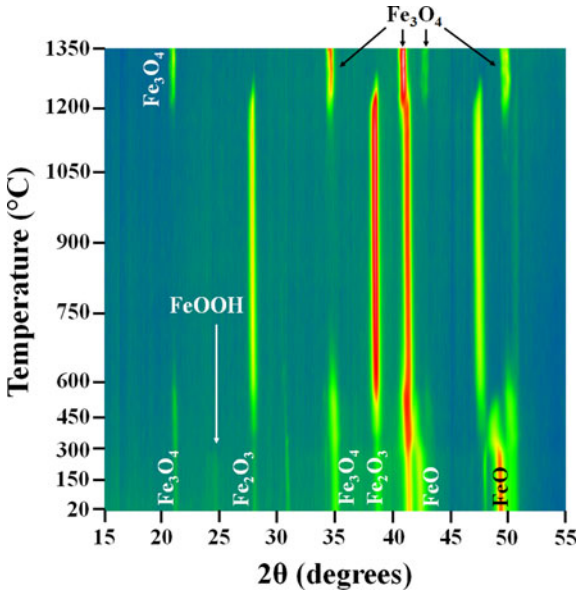

Figure 1. (Colour online) *In situ* XRD data collected for the mill scale sample, viewed down the intensity axis, over the range 20–1350 °C at $pO_2 = 5 \times 10^{-3}$ atm.

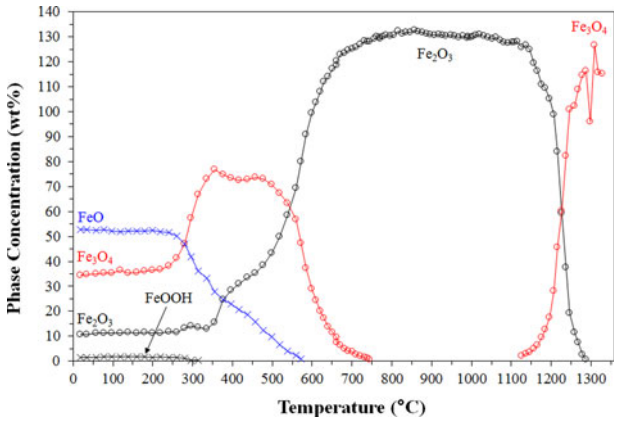

Figure 2. (Colour online) Results of Rietveld-based quantitative phase analysis, showing absolute phase concentrations as a function of temperature, for the mill scale sample.

https://doi.org/10.1017/S088571561700080X Published online by Cambridge University Press

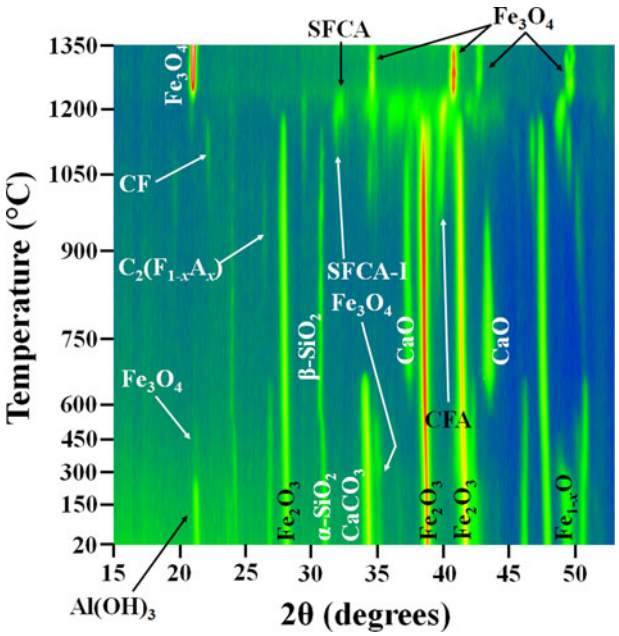

Figure 3. (Colour online) *In situ* XRD data collected for the 21.2 wt% mill scale mixture.

Figure 4 shows stack plots of the *in situ* XRD collected for the 2.6, 10.6, and 21.2 wt% mixtures in the range 1100–1310 °C. Indeed, the effect of increasing mill scale concentration of the formation of the SFCA-I and SFCA phases does appear to be minimal. This is attributed, firstly, to the low impurity (i.e. Mg, Mn) content in the mill scale. Secondly, any Fe_2O_3 which forms through oxidation of the FeO and Fe_3O_4 in the mill scale only begins to convert to Fe_3O_4 above ~1150 °C (see Figures 1 and 2) and so no appreciable conversion of Fe_2O_3 to Fe_3O_4, which is unreactive in the context of SFCA-I and SFCA phase formation (Webster *et al*., 2013a), can occur before formation of SFCA-I and SFCA and the Fe_2O_3 is available for reaction to form the SFCA phases. If the pO_2 the experiments were conducted under was more reducing, then the effect of mill scale addition would likely become significant, in accordance with the results of Wang *et al*. (2016b).

IV. CONCLUSION

The thermal decomposition of mill scale, and the effect of mill scale addition on the formation and decomposition of SFCA-I and, has been investigated using *in situ* XRD. Application of the external standard method to the QPA of the *in situ* data collected during decomposition of the mill scale highlighted the applicability of this method for the determination of the nature and abundance of amorphous material in a mineral sample; the mill scale was shown to contain 33 wt% of amorphous Fe-oxide material. Increasing mill scale addition from 2.6 to 10.6 and to 21.2 wt% did not significantly affect the thermal stability ranges of SFCA-I or SFCA, nor did it significantly affect the amount of each of SFCA or SFCA-I which formed. This was attributed to the low impurity (i.e. Mn, Mg) concentration in the mill scale, and also the transformation to hematite during heating of the wüstite and magnetite present in the mill scale under ambient conditions, with the hematite available for reaction to form SFCA and SFCA-I.

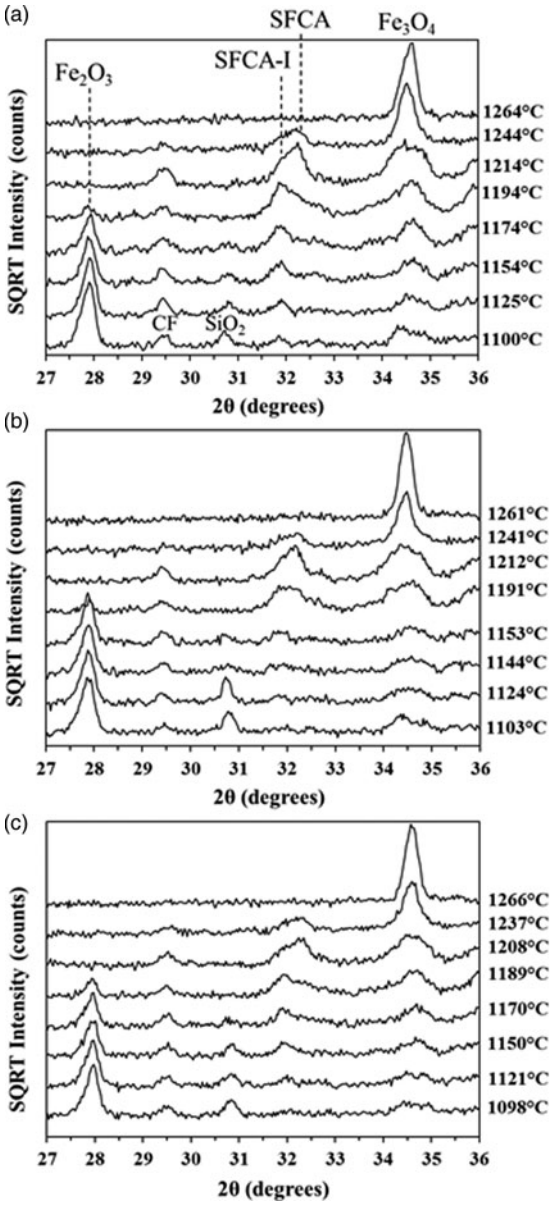

Figure 4. Stack plots of the *in situ* XRD collected for the (a) 2.6, (b) 10.6, and (c) 21.2 wt% mixtures in the range 1100–1310 °C. Datasets are offset in the vertical axes for clarity. The temperature values provided are those at the start – which is when the temperatures were automatically recorded – of the datasets. Reflections for key phases are marked in (a).

ACKNOWLEDGEMENT

The authors thank Dr. Zhe Wang (University of Wollongong) for providing the mill scale sample.

Ahsan, S. N., Mukherjee, T., and Whiteman, J. A. (**1983**). "Structure of fluxed sinter," Ironmak. Steelmak. **10**, 54–64.

Birks, N., Meier, G. H., and Pettit, F. S. (**2006**) *Introduction to the High Temperature Oxidation of Metals* (Cambridge University Press, Cambridge), 2nd ed.

Blake, R., Hessevick, R., Zoltai, T., and Finger, L. (**1966**). "Refinement of the hematite structure," Am. Mineral. **51**, 123–129.

Bruker (**2014**). TOPAS, version 5. Bruker AXS Inc., Madison, Wisconsin, USA.

Dawson, P. R., Ostwald, J., and Hayes, K. M. (**1985**). "Influence of alumina on the development of complex calcium ferrites in iron ore sinters," T. I. Min. Metall. C **94**, 71–78.

https://doi.org/10.1017/S088571561700080X Published online by Cambridge University Press

Fjellvåg, H., Grønvold, F., Stølen, S., and Hauback, B. C. (**1996**). "On the crystallographic and magnetic structures of nearly stoichiometric iron monoxide," J. Solid State Chem. **124**, 52–57.

Hamilton, J. D. G., Hoskins, B. F., Mumme, W. G., Borbidge, W. E., and Montague, M. A. (**1989**). "The crystal structure and crystal chemistry of $Ca_{2.3}Mg_{0.8}Al_{1\cdot5}Si_{1.1}Fe_{8.3}O_{20}$ (SFCA): solid solution limits and phase relationships of SFCA in the SiO_2-Fe_2O_3-CaO(-Al_2O_3) system," Neues Jahrb. Miner. Abh. **161**, 1–26.

Hamilton, W. C. (**1958**). "Neutron diffraction investigation of the 119 K transition in magnetite," Phys. Rev. **110**, 1050–1057.

Hancart, J., Leroy, V., and Bragard, A. (**1967**). *A Study of the Phases Present in Blast Furnace Sinter. Some Considerations on the Mechanism of their Formation* (C.N.R.M. Report, DS 24/67), pp. 3–7.

Hazemann, J. L., Berar, J. F., and Manceau, A. (**1991**). "Rietveld studies of the aluminium-iron substitution in synthetic goethite," Mater. Sci. Forum **79**, 821–826.

Hill, R. J. and Howard, C. J. (**1987**). "Quantitative phase analysis from neutron powder diffraction data using the Rietveld method," J. Appl. Crystallogr. **20**, 467–474.

Hsieh, L-H. and Whiteman, J. A. (**1989**). "Sintering conditions for simulating the formation of mineral phases in iductrial iron ore sinter," ISIJ Int. **29**, 24–32.

Huebner, J. S. (**1971**). "Buffering techniques for hydrostatic systems at elevated pressures," in *Research Techniques for High Pressure and High Temperature*, edited by G. C. Ulmer (Springer-Verlag, New York), pp. 123–178.

Lager, G. A., Jorgensen, J. D., and Rotella, F. J. (**1982**). "Crystal structure and thermal expansion of α-quartz SiO_2 at low temperature," J. Appl. Phys. **53**, 6751–6756.

Li, Y., Li, Y. Q., and Fruehan, R. J. (**2001**). "Formation of titanium carbonitride from hot metal," ISIJ Int. **41**, 1417–1422.

Madsen, I. C. and Scarlett, N. V. Y. (**2008**). "Quantitative phase analysis," in *Powder Diffraction: Theory and Practice*, edited by R. E. Dinnebier and S. J. L. Billinge (Royal Society of Chemistry, Cambridge), pp. 298–331.

Minervini, L. and Grimes, R. W. (**1999**). "Defect clustering in wüstite," J. Phys. Chem. Solids **60**, 235–245.

Mumme, W. G., Clout, J. M. F., and Gable, R. W. (**1998**). "The crystal structure of SFCA-I, $Ca_{3.18}Fe^{3+}_{14.66}Al_{1\cdot34}Fe^{2+}_{0.82}O_{28}$, a homologue of the aenigmatite structure type, and new crystal structure refinements of β-CFF, $Ca_{2.99}Fe^{3+}_{14.30}Fe^{2+}_{0.55}O_{25}$ and Mg-free SFCA, $Ca_{2.45}Fe^{3+}_{9.04}Al_{1\cdot74}Fe^{2+}_{0.16}Si^{0\cdot6}O_{20}$," Neues Jahrb. Miner. Abh. **173**, 93–117.

Patrick, T. R. C. and Pownceby, M. I. (**2001**). "Stability of SFCA (silico-ferrite of calcium and aluminium) in air: solid solution limits between 1240 °C and 1390 °C and phase relationships within the Fe_2O_3-CaO-Al_2O_3-SiO_2 (FCAS) system," Metall. Mater. Trans. B **32**, 1–11.

Shannon, R. D. (**1976**). "Revised effective ionic radii and systematic studies of interatomic distances in halides and chalcogenides," Acta Crystallogr. A Cryst. **32**, 751–767.

Umadevi, T., Brahmacharyulu, A., Karthik, P., Mahapatra, P. C., Prabhu, M., and Ranjan, M. (**2012**). "Recycling of steel plant mill scale via iron ore sintering plant," Ironmak. Steelmak. **39**, 222–227.

Wang, Z., Pinson, D., Chew, S., Rogers, H., Monaghan, B. J., Pownceby, M. I., Webster, N. A. S., and Zhang, G. (**2016a**). "Behaviour of New Zealand Ironsand during iron ore sintering," Metall. Mater. Trans. B **47**, 330–343.

Wang, Z., Pinson, D., Chew, S., Monaghan, B. J., Pownceby, M. I., Webster, N. A. S., Rogers, H., and Zhang, G. (**2016b**). "Effect of addition of mill scale on sintering of iron ores," Metall. Mater. Trans. B **47**, 2848–2860.

Webster, N. A. S., Pownceby, M. I., Madsen, I. C., and Kimpton, J. A. (**2012**). "Silico-ferrite of calcium and aluminium (SFCA) iron ore sinter bonding phases: new insights into their formation during heating and cooling," Metall. Mater. Trans. B **43**, 1344–1357.

Webster, N. A. S., Pownceby, M. I., Madsen, I. C., and Kimpton, J. A. (**2013a**). "Effect of oxygen partial pressure on the formation mechanisms of complex Ca-rich ferrites," ISIJ Int. **53**, 774–781.

Webster, N. A. S., Pownceby, M. I., and Madsen, I. C. (**2013b**). "*In situ* X-ray diffraction investigation of the formation mechanisms of silico-ferrite of calcium and aluminium-I-type complex calcium ferrites," ISIJ Int. **53**, 1334–1340.

Webster, N. A. S., Pownceby, M. I., Madsen, I. C., Studer, A. J., Manuel, J. R., and Kimpton, J. A. (**2014**). "Fundamentals of SFCA (Silico-ferrite of Calcium and Aluminium) and SFCA-I iron ore sinter bonding phase formation: effects of CaO:SiO_2 ratio," Metall. Mater. Trans. B **45**, 2097–2105.

Webster, N. A. S., Churchill, J. G., Tufaile, F., Pownceby, M. I., Manuel, J. R., and Kimpton, J. A. (**2016**). "Fundamentals of silico-ferrite of calcium and aluminium (SFCA) and SFCA-I iron ore sinter bonding phase formation: effects of titanomagnetite-based ironsand and titanium addition," ISIJ Int. **56**, 1715–1722.

Webster, N. A. S., O'Dea, D. P., Ellis, B. G., and Pownceby, M. I. (**2017**). "Effects of gibbsite, kaolinite and al-rich goethite as alumina sources on silico-ferrite of calcium and aluminium (SFCA) and SFCA-I iron ore sinter bonding phase formation," ISIJ Int. **57**, 41–47.

https://doi.org/10.1017/S088571561700080X Published online by Cambridge University Press